Abundant polymorphic transitions in the $Al_{0.6}CoCrFeNi$ high-entropy alloy

HPSTAR
687-2019

L. Wang [a, b], F. Zhang [c, d], Z. Nie [a], L. Wang [a], F. Wang [a], B. Wang [a], S. Zhou [a], Y. Xue [a, *], B. Cheng [c], H. Lou [c], X. Chen [c], Y. Ren [f], D.E. Brown [b], V. Prakapenka [g], E. Greenberg [g], Z. Zeng [c], Q.S. Zeng [c, e, **]

[a] School of Materials Science and Engineering, Beijing Institute of Technology, Beijing 100081, People's Republic of China
[b] Department of Physics, Northern Illinois University, Dekalb, IL 60115, USA
[c] Center for High Pressure Science and Technology Advanced Research, Pudong, Shanghai 201203, People's Republic of China
[d] State Key Laboratory for Advanced Metals and Materials, University of Science and Technology Beijing, Beijing 100083, People's Republic of China
[e] Jiangsu Key Laboratory of Advanced Metallic Materials, School of Materials Science and Engineering, Southeast University, Nanjing 211189, People's Republic of China
[f] X-ray Science Division, Argonne National Laboratory, Argonne, IL 60439, USA
[g] Center for Advanced Radiation Sources, University of Chicago, Chicago, IL 60437, USA

ARTICLE INFO

ABSTRACT

Polymorphism and polymorphic transitions are attracting considerable interest because of their significant effect on the phase stability, switchable properties, and the atomic rearrangement mechanism in materials. Here, by employing *in situ* high-pressure synchrotron radiation X-ray diffraction, we reveal surprisingly abundant polymorphic transitions in an $Al_{0.6}CoCrFeNi$ high-entropy alloy (HEA). The original body-centered cubic (*bcc*) phase transfers to an orthorhombic phase at ~ 10.6 GPa during compression at room temperature, and the orthorhombic phase remains stable up to ~ 40 GPa. When the lattice stress is released entirely, the orthorhombic phase can further transform into a body-centered tetragonal structure. On the other hand, when the original *bcc* phase is heated to high temperatures, a face-centered cubic phase forms, and it can further transform to a hexagonal close packing phase by applying pressure. In total, we observed five polymorphs in the Al06 HEA, and they all can exist at ambient conditions. The complex chemistry and the pressure/temperature tuned lattice distortion may play a key role in introducing and stabilizing the rich polymorphs in the Al06 HEA. Our findings may bring new insights into the correlation between lattice distortion and phase stability/transitions of HEAs and help to explore HEAs with novel structures and properties.

1. Introduction

Polymorphism, the ability of a material with an identical composition to exist in more than one crystal structure, has been extensively observed in a vast amount of materials including pure elements [1—12], compounds [13—18], and alloys [19—21]. Polymorphs with different structures can be readily altered by temperature- and/or pressure-induced polymorphic transitions. The

study of polymorphism is crucial to understand the phase stability/transitions, the mechanism of the atomic arrangement, and also to achieve switchable functions in properties such as the optical [22], electrical [23,24], and mechanical [12,25—28] properties.

In the periodic table, the biggest group of elements is the metals, which typically own a simple close-packed structure due to their non-directional metallic bonds, such as body-centered cubic (*bcc*), face-centered cubic (*fcc*), and hexagonal close packing (*hcp*) structures. Pressure is a powerful tuning parameter to induce polymorphic transitions between those structures in metals. One of the most famous examples is iron, which shows three well-established polymorphs with *fcc*, *hcp*, or *bcc* structures. The polymorphic transitions between these polymorphs of iron have been widely studied under both static [4,7,12,19,25,29—32] and shock

compression [33,34]. Usually, less than three polymorphs exist in a metal element, and its polymorphic transitions are mostly reversible [4,7,12,19,25,29–32,35–38]. Some typical polymorphic transitions in metal elements are listed in Table 1. Pursuing new polymorphs in these pure elements by pushing the pressure and temperature limit to unexplored regions has been a major focus [7,19,30,35,39].

Adding metallic elements into another (solvent) with appropriate ratios could lead to the formation of solid solutions, namely metallic alloys. These alloys could possess properties much superior to each individual component. Therefore, since the Bronze and Iron Ages, the development of metallic alloys have played a crucial role in the advancement of civilizations. The most common type of alloy is the substitutional solid solution in which solute atoms randomly substitute for atoms in the solvent lattice. Thus, the alloys usually inherit the initial crystal structure of the solvent (principal) elements and are also typically named after the solvent, such as Fe-based, Al-based, and Ti-based alloys, etc. In traditional metallurgy, when more and more elements are added to a solution, precipitation of various intermetallic compounds readily occurs and results in the embrittlement of the materials. Therefore, traditional alloys are mainly located at the corner of their multicomponent phase diagrams to avoid forming brittle composites.

Over the last decade, high-entropy alloys (HEAs) [40–42] based on a new alloy design concept have been developed by deliberately incorporating five or more elements with equimolar or near-equimolar ratios to maximize their configurational entropy. As a result, these new alloys can be surprisingly stabilized into single solid solution phases with a simple crystal structure, such as the *fcc* [43,44], *bcc,* [27,45] and *hcp* [46]. Owing to their unique compositions, high chemical disorder, and severe local lattice distortion, HEAs present high thermal stability, high wear and corrosion resistance, and promising mechanical properties [28,42,43,47–50].

It is not surprising that polymorphism is common in traditional metallic alloys, which mostly inherit the polymorphic transitions of their solvent elements [7,19,51,52]. However, whether this kind of polymorphism is still possible in the HEAs with multiple-principal components, but no identifiable solvent has been an intriguing open question. Previous studies [53–55] showed that during heating from cryogenic temperature up to melting temperature, no polymorphic transition was observed in the CoCrFeNiMn HEA system. The exceptional phase stability was attributed to their high configurational entropy as well as the chemical disorder and considerable local lattice distortion induced by the chemical complexity [56–61]. Very recently, under high pressure, it was

discovered that the CrMnFeCoNi HEA [62–64] and the NiCoCrFe HEA [65] exhibit *fcc*-to-*hcp* polymorphic phase transitions. These results suggest that the HEAs may be far more complex than simply 'highly-stable' as we expected, especially with applying high pressure. Is polymorphism general to HEAs with various initial structures? Besides *fcc* and *hcp* structures, is there any polymorphism in the *bcc* HEAs under high pressure? How flexible can an HEA structure be? Are multipolymorphs possible in HEA systems? The answers to these questions are vital to understanding the phase stability and transitions of HEAs and exploration of new HEA materials.

In this study, Al$_{0.6}$CoCrFeNi HEA powders (Al06) with a single *bcc* phase were prepared by gas atomization, and the structure at high pressure was investigated by employing *in situ* high-pressure synchrotron radiation X-ray diffraction (XRD) in a diamond anvil cell (DAC). We discovered a *bcc*-to-orthorhombic phase transition in the gas-atomized Al06 sample, which started at ~10.6 GPa and completed at ~21.4 GPa. When the pressure was totally released, body-centered tetragonal (*bct*) phase was found to co-exist with the orthorhombic phase, showing that the start pressure of the orthorhombic-to-*bct* transition is close to the ambient pressure. Moreover, after annealing the gas-atomized *bcc* Al06 at 1000°C for 2 h, a more stable *fcc* phase was obtained. The *fcc* phase completely transformed to an *hcp* phase during compression. We suggest severe lattice distortion manipulated by temperature and high pressure may play a crucial role in controlling the formation of various polymorphs in the Al06 HEA. In total, five polymorphs were obtained that could all exist at ambient conditions. These results demonstrate that HEAs could have structural flexibility far beyond that of their constituent elements, opening up an avenue toward unexplored region for HEAs design and development.

2. Materials and methods

2.1. Sample preparation

The Al0.6CoCrFeNi (Al06) HEA ingots were prepared by arc melting a mixture of high-purity metals (>99.9 mass %) in a Ti-gettered high-purity Ar atmosphere. Each ingot was re-melted at least four times to ensure chemical homogeneity. Al06 powders were prepared by high-pressure argon gas atomization. The master ingots were heated up to 1600°C under high vacuum conditions (<10^{-2} Pa). Subsequently, the molten alloy was injected through a nozzle into droplets by Ar with a pressure of 3.5 MPa. Powders between 25 and 38 μm were then sieved for further investigation.

Table 1
Some typical pressure-induced polymorphic transitions in the metal elements and alloys.

Metal/alloy	Phase transition	Transition initial pressure	Reversibility	Ref
Al	*fcc*→*hcp*→*bcc*	216 GPa (*hcp*) 321 GPa (*bcc*)	–	[1]
Fe	*bcc*→*hcp*	14.7 GPa	Reversible	[4,7,12,19,25,29–32]
V	*bcc*→Rhombohedral	63–69 GPa	–	[8]
Co	*hcp*→*fcc*	105 GPa	Reversible	[26,35]
Ti	*hcp*(α)→Distorted *bcc*(ω)→Orhorthombic(γ)	116 GPa (γ)	Reversible	[36]
Zr	*hcp*(α)→Distorted *bcc*(ω)→*bcc*(β)	30 GPa (β)	Reversible	[35]
Hf	*hcp*(α)→Distorted *bcc*(ω)→*bcc*(β)	50 GPa (ω) 60.5 GPa (β)	Reversible	[5]
Na	*bcc*→*fcc*	65 GPa	–	[81]
Pb	*fcc*→*hcp*	13 GPa	–	[82]
Ge	Ge_I→Ge_II→Ge_III	10.5 GPa (Ge_II)	Reversible	[83]
CoCrFeNiMn	*fcc*→*hcp*	7–22 GPa	Irreversible	[62–64]
CoCrFeNi	*fcc*→*hcp*	13.5 GPa	Irreversible	[65]
Al$_{0.6}$CoCrFeNi	*fcc*→*hcp*, *bcc*→Orhorthombic(O)→*bct*	10.6 GPa (*hcp*) 10.6 GPa (O) lattice stress release (*bct*)	Irreversible	This work

bcc, body-centered cubic; *bct*, body-centered tetragonal; *fcc*, face-centered cubic; *hcp*, hexagonal close packing.

2.2. In situ high-pressure synchrotron radiation XRD

In situ high-pressure angle-dispersive XRD experiments were performed at beamline 13-ID-D, Advanced Photon Source, Argonne National Laboratory. An X-ray beam with a wavelength of 0.322 Å and a beam size of 2.5 μm × 3 μm was used during the tests. The detector position and orientation were calibrated using the LaB$_6$ standard. A DAC with a 400 μm diameter culet was used to generate high pressures. A T301 stainless steel gasket was preindented down to a thickness of ~42 μm. A 150 μm hole was drilled as a sample chamber at the center of the gasket indent by a laser drilling system. The gas-atomized Al06 powder with a diameter of ~20 μm was loaded into the DAC, and a tiny ruby ball beside the sample was used as a pressure calibrant. Silicone oil was used as the pressure-transmitting medium. Two-dimensional (2D) diffraction patterns were collected using a Mar165 charge-coupled device detector, and the exposure time was set at 2s. 2D diffraction patterns were integrated by the Dioptas software [66], and the results were refined using the GSAS package [67].

2.3. Microstructure characterization

The microstructure of the samples was examined by a Hitachi S4800 scanning electron microscope (SEM) with an energy dispersive spectrometer (EDS) and JEOL JEM-2100 transmission electron microscope (TEM) with selected area electron diffraction (SAED). The TEM samples were prepared by focused ion beam (FIB, FEI Versa 3D).

3. Results

3.1. Microstructure at ambient pressure

The Al06 sample synthesized by gas atomization is a *bcc* (B2 or A2) phase (Supplementary Fig. S1a) with a unit cell parameter of a = 2.864 (2) Å. Since the B2 phase (space group: *Pm-3m*) and A2 phase (space group: *Im-3m*) are only different in the chemical ordering but have identical unit cell parameters, here, the gas-atomized Al06 could be treated simply as a single *bcc* phase HEA for convenience. The spherical particle powders are polycrystalline with a grain size ranging from submicron to a few microns (Supplementary Fig. S1b). The energy-dispersive X-ray spectroscopy analysis confirmed that the composition of gas-atomized Al06 is homogeneous and close to the nominal composition (Supplementary Fig. S2a).

3.2. High pressure—induced phase transitions

In situ high-pressure XRD experiments of the gas-atomized Al06 were investigated in a DAC up to ~40.4 GPa (Supplementary Fig. S3). The XRD patterns during loading and unloading are shown in Fig. 1a. With increasing pressure, the diffraction peaks shift to higher 2-theta values. When the pressure approached ~10.6 GPa, a new diffraction peak beside the *bcc* (110) peak appears, suggesting the occurrence of a phase transition. With further pressure increase, more new diffraction peaks emerge and increase their peak intensity appreciably at the expense of the initial *bcc* peaks, and the initial *bcc* peaks almost entirely disappear at ~21.4 GPa, indicating the completion of the phase transition. During the unloading process, the *bcc* phase does not reappear, and the newly formed phase seems retained.

To identify the structure of the new phase, the high-pressure XRD patterns were fitted using the Le Bail method in the GSAS package [67]. Although the new peaks look quite similar to that of an *hcp* phase as observed in the Cantor's alloy [62,63], the XRD pattern actually cannot be well-fitted by an *hcp* phase. In contrast, all new phase peaks can be well indexed into an orthorhombic (space group *Cmcm*) phase (Supplementary Fig. S4a and b). Similar pressure- or deformation-induced *bcc* to orthorhombic phase transitions were reported in other metals [51,68,69]. Therefore, it suggests that a transition from *bcc* to orthorhombic phase at high-pressure is observed in the Al06 HEA.

The *bcc* Al06 powder in this work was synthesized using the gas-atomization method, which produces microsized particles with much higher cooling rate than the typical melt-casting method. Therefore, a single *bcc* structure rather than the typical *fcc* (main) + *bcc* biphasic mixture [70—72] (usually obtained by casting) was obtained in the Al06 powders. After annealing the gas-atomization Al06 powders at 1000°C for 2 h, the *bcc* phase transformed into a more stable *fcc* phase (Supplementary Fig. S1a and c). When we compressed the annealed Al06 powders to high pressures (loaded in the same DAC together with the as-prepared *bcc* sample), a sluggish and irreversible *fcc*-to-*hcp* phase transition was observed (Fig. 1b), which is similar to the behavior of its master alloy CoCrFeNi [65].

According to the refinement results, the average volume per atom for the *bcc*, orthorhombic, *fcc,* and *hcp* phases was calculated, as shown in Fig. 2a. Volume collapse appeared in the *bcc*-to-orthorhombic phase transition, which is only 27% of the full volume collapse value as that in the *bcc*-to-*hcp* phase transition observed in
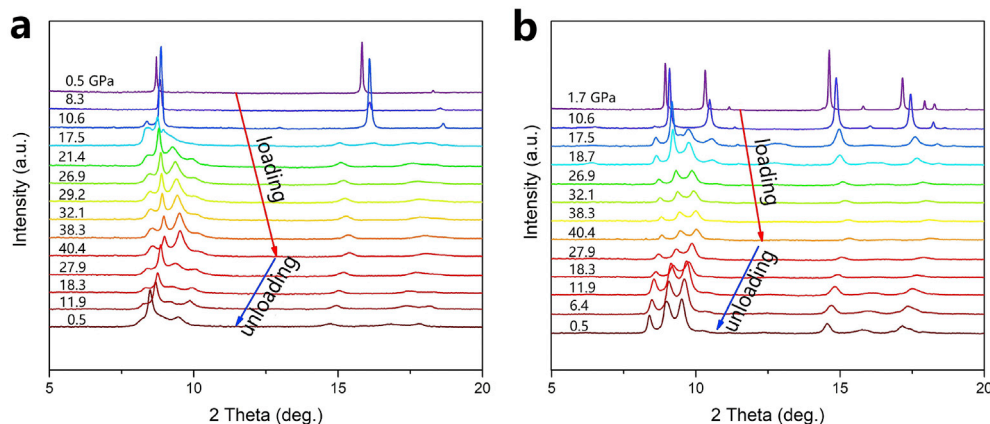

Fig. 1. The *in situ* high-pressure XRD patterns of the Al06 HEA. (a) XRD patterns at different pressures of the *bcc* Al06 HEA during loading and unloading. A phase transition starts at ~10.6 GPa and completes at ~21.4 GPa. (b) XRD patterns at different pressures of the *fcc* Al06 HEA during loading and unloading. The X-ray wavelength is 0.322 Å. Please note that the grain size in the *bcc* Al06 powders is not small enough to obtain a smooth diffraction ring (Supplementary Figs. S1b and S4b). Therefore, the relative intensity of the *bcc*/orthorhombic peaks is not statistically reliable. XRD, X-ray diffraction; *bcc*, body-centered cubic; HEA, high-entropy alloy; *fcc*, face-centered cubic.
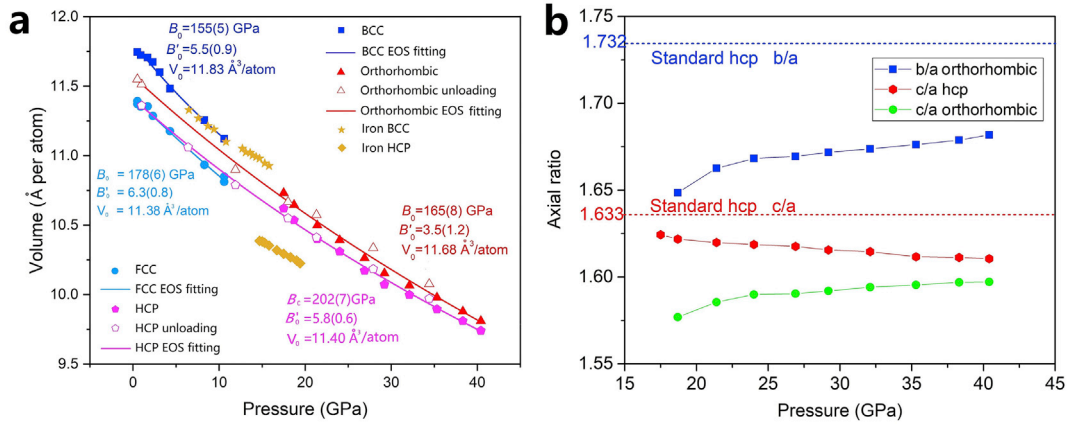
Fig. 2. The atomic volume and unit cell parameter changes as a function of pressure through the phase transitions. (a) The atomic volume changes of Al06 HEAs as a function of pressure during loading and unloading. The volume data were fitted by a third-order Birch-Murnaghan isothermal equation of state (EOS) [73], and the ambient pressure volume (V_0) and bulk moduli (B_0) at ambient pressure were determined. The khaki stars are the volume data of iron with a *bcc*-to-*hcp* phase transition at high pressures [4]. (b) The *b/a* and *c/a* ratio variation in the gas-atomized and annealed Al06 HEAs during loading. *bcc*, body-centered cubic; HEA, high-entropy alloy; *fcc*, face-centered cubic.

iron [4]. The volume data can be well-fitted by a third-order Birch-Murnaghan isothermal equation of state [73], and the ambient-pressure volume (V_0) and bulk moduli (B_0) at ambient pressure were determined (Fig. 2a). The ambient pressure bulk moduli B_0 of the *bcc* and orthorhombic phases of the gas-atomized Al06 HEA are 155 (5) GPa and 165 (8) GPa, respectively, which are quite consistent with the previous experimental and simulation results [72,74]. The volume (V_0) per atom of the *bcc* phase and orthorhombic phase are 11.83 Å³/atom and 11.68 Å³/atom, respectively. Compared with the initial *bcc* phase, the orthorhombic phase has increased density (by ~1.3%) and bulk modulus (by ~ 6.5%). In the annealed Al06, the ambient pressure volume (V_0) per atom of the *fcc* and *hcp* phases are 11.38 Å³/atom and 11.40 Å³/atom, respectively. No volume collapse appeared in the *fcc*-to-*hcp* phase transition, consistent with previous works [62,63,65]. Fig. 2b shows the comparison of the unit cell parameter ratio (*b/a* and *c/a*) of different polymorphs of Al06 during compression.

It should be noted that the orthorhombic phase Al0.6 HEA can be almost fully retained down to ~0.5 GPa. However, once the pressure was totally released down to 0 GPa, a new peak at ~8.85° was found (Supplementary Fig. S4e and f). The (110) peak of the *bcc* phase is at ~9.11° at ambient pressure, indicating that the new peak should not come from the *bcc* phase. To identify the structure of the new phase, the XRD pattern at 0 GPa after decompression was fitted

using the Le Bail method in the GSAS package, as shown in Fig. S4e and f. The XRD pattern could be well-fitted by an orthorhombic + *bct* biphasic structure. The new peak at ~8.85° was confirmed to be the (110) peak of the *bct* phase, with $a = 2.93$ (3) Å and $c = 2.80$ (3) Å.

3.3. TEM characterization

The gas-atomized initial Al06 HEA before and after the high-pressure experiment (decompressed from ~41 GPa) was further investigated by TEM. The TEM images and the SAED are shown in Fig. 3. The TEM samples were prepared by FIB (FEI Versa 3D) technology. As shown in Fig. 3a, the gas-atomized initial Al06 HEA has a *bcc*/B2 structure with a unit cell parameter of $a = 2.85$ (1) Å, consistent with the XRD results (Supplementary Fig. S1a). In Fig. 3b, rather than the orthorhombic + *bct* biphasic structure revealed by *in situ* high-pressure XRD, the TEM measurement of the high-pressure recovered Al06 sample surprisingly shows a single *bct* structure, with the unit cell parameter of $a = 2.95$ (1) Å and $c = 2.83$ (1) Å. The SEM images of the TEM samples are shown in Supplementary Fig. S5. Compared with the flat gas-atomized initial Al06 TEM sample, the high-pressure-recovered Al06 TEM sample is quite waved, suggesting that considerable lattice stress may still partially exist in the high-pressure-recovered sample, then the
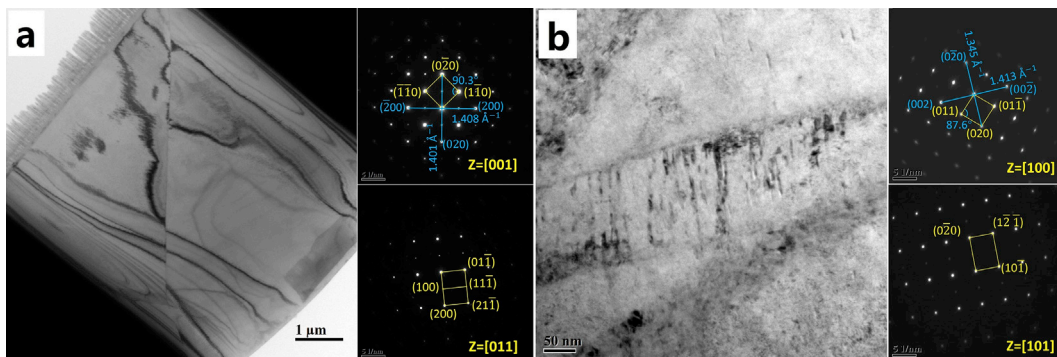

Fig. 3. TEM and SAED patterns of the gas-atomized Al06 powder before (a) and after (b) the high-pressure experiment. The SAED in (a) shows a typical *bcc*/B2 structure and the lattice constant is calculated to be $a = 2.85$ (1) Å. In (b), the distance between (020) and (0$\bar{2}$0) is 1.345 Å⁻¹, obviously smaller than that between (002) and (00$\bar{2}$), which is 1.413 Å⁻¹. Instead of a right angle, the angle (000)-to-(011)-to-(020) is 87.6°. All these characteristics show that the phase in the gas-atomized Al06 after high-pressure experiment is a typical *bct* phase, and the lattice constants are calculated to be $a = 2.95$ (1) Å and $c = 2.83$ (1) Å. TEM, transmission electron microscope; SAED, selected area electron diffraction; *bcc*, body-centered cubic; *bct*, body-centered tetragonal.

stress further releases during FIB cutting/thinning (probably deconfinement effect) and causes deformation. The TEM results indicate that the orthorhombic phase in the high-pressure released Al06 powder is metastable and may be kept by the residual lattice stress. After the FIB cutting process, the lattice stress was relaxed and then the orthorhombic + bct biphasic can fully transform to the bct phase.

4. Discussion

The phase stability of the Al$_x$CoCrFeNi HEA system has been widely studied at ambient conditions. The master quaternary alloy CoCrFeNi has an fcc phase as the well-known Cantor's alloy (CoCrFeNiMn). By adding Al atoms into the CoCrFeNi master alloy with increasing content, the Al$_x$CoCrFeNi HEA changes from a single fcc phase (x < ~0.5), through fcc + bcc co-existing phases (~0.5 < x < ~0.9), to a single bcc phase (x > ~0.9) [42,43,47]. The main reason is that the Al atom size is much larger than the other four elements; the increasing lattice distortion caused by Al alloying changes the phase stability of Al$_x$CoCrFeNi [42,75]. The Al06 composition studied in this work is located around the boundary between the fcc and the fcc + bcc phases. Therefore, the Al06 HEA may be susceptible to changes in external conditions or tuned with possible rich polymorphism. Al06 HEA powder could be prepared by using the gas-atomization method. The particles with small size (diameter < 75 μm) shows a single bcc phase, and the particles with large size (diameter > 75 μm) shows a fcc + bcc mixture phase [70]. The smaller size means the faster cooling rate. During the fast quenching, the atom diffusion would be restricted by limited time window for atoms to move to a more favorable position, and excess energy would be stored in the atomic structure in terms of relative large lattice distortion. Similar to the effect of increasing concentration of Al in the AlxCoCrFeNi HEA system, accumulated high lattice distortion may cause the forming of a bcc structure. Thus, the lattice distortion could be controlled by manipulating the atom diffusion as well. Further annealing of the bcc Al06 HEA at high temperature enhances the atom diffusion. Therefore, the bcc phase

transformed into a more stable fcc phase with reduced lattice distortion. When we compressed the annealed Al06 samples to high pressures, an irreversible fcc to hcp phase transition was observed, which is similar to the behavior of its master alloy CoCrFeNi [65]. In contrast, the gas-atomized initial Al06 powders without annealing showed a bcc-to-orthorhombic phase transition during compression. After the lattice stress fully released in the decompressed gas-atomized Al06, the orthorhombic phase totally transformed to a single bct phase. These unusually rich polymorphism phenomena including five polymorphs (Fig. 4) have never been predicted or experimentally observed in any HEA. How and why did the bcc phase in the gas-atomized initial Al06 HEA transform to an orthorhombic instead of a more stable high-pressure hcp phase? Why does the orthorhombic phase further transform into a bct phase? These are key issues for further understanding the phase stability of Al06 HEA and its rich polymorphism.

4.1. Phase transition mechanism

The high pressure−induced bcc-to-hcp phase transition has been intensely studied in iron [12,25,30−33,68]. As stated by Mao et al. [12] and Bassett et al. [31], the hcp structure of iron can be derived through a relatively minor distortion of its bcc structure during compression. An orthorhombic phase can usually be considered as a distorted hcp phase [68]. As shown in Fig. 5, with the pressure increase, the bcc lattice contracts along the [001] direction on the (110) plane and expands along the [1$\bar{1}$0] direction. An additional shuffling of the alternate (110) planes of the initial bcc phase can readily establish the atomic ordering of an orthorhombic phase with $\sqrt{2}a < b < \sqrt{3}a$ or further an hcp lattice with $b = \sqrt{3}a$. In the Al06 HEA, the structure seems to get stuck halfway through the bcc-to-hcp transition, synthesizing the orthorhombic phase. Thus, the volume collapse in the bcc-to-orthorhombic phase transition (Fig. 2a) is not as thorough as that in the bcc-to-hcp phase transition in iron [4]. As mentioned previously, the bcc structure is a metastable phase trapped by the fast quenching rate in the gas-
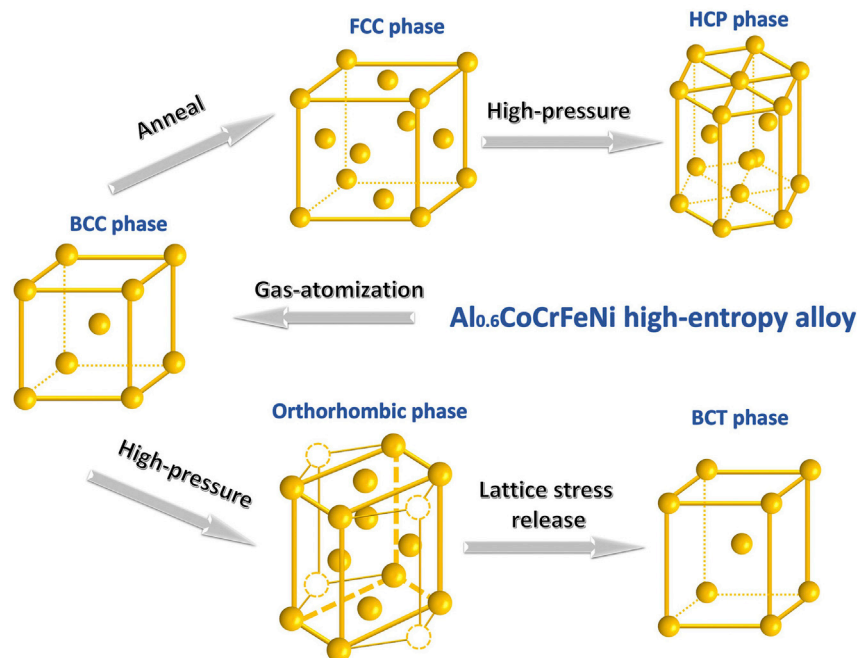

Fig. 4. The schematic plot of the atomic structure and transition paths between all five polymorphs of the Al06 HEA. *bcc*, body-centered cubic; *bct*, body-centered tetragonal; *fcc*, face-centered cubic; *hcp*, hexagonal close packing.
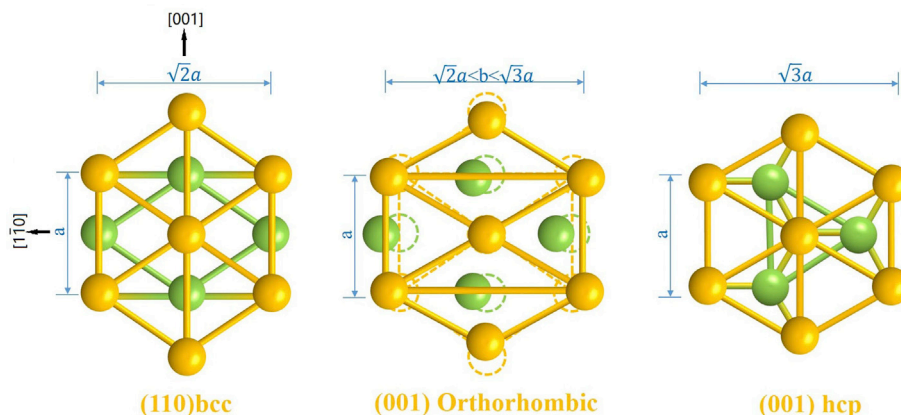
Fig. 5. Schematic plot of the lattice relationship between the *bcc*, orthorhombic, and *hcp* structures and the possible transition mechanism. During the transition, the *bcc* lattice was contracted along the [001] direction and expanded along the [1$\bar{1}$0] direction, lattice distortion hindered the atom movements, and the structure may get stuck halfway to the *hcp* phase, synthesizing an orthorhombic phase. *bcc*, body-centered cubic; *hcp*, hexagonal close packing.

atomization process. Compared with the *fcc* phase obtained by melt-casting, it is reasonable to expect that more severe lattice distortion may be quenched in the *bcc* phase because of less time available for atoms to adjust their positions toward a more comfortable arrangement (the *fcc* phase). During the compression of the *bcc* Al06 HEA, unlike the case of pure iron, the lattice distortion in the Al06 HEA hinders the atom movements and eventually results in the formation of a metastable orthorhombic phase, which can be mostly retained to ambient conditions with minor *bct* phase. However, once the lattice stress in Al06 is further released after FIB cutting (removal of the confinement caused by surrounding bulk materials), the remaining orthorhombic phase transformed to a *bct* phase. This phenomenon indicates that under ambient conditions, the *bcc* phase is still more stable than the orthorhombic phase, and the latter tends to transform into the former. However, like the high-pressure transition, the orthorhombic-to-*bcc* is hindered halfway as well, synthesizing the *bct* structure instead.

4.2. Correlation between lattice distortion and phase transition

Compared with temperature, pressure is a more powerful external parameter for squeezing the volume, altering the atom arrangement and the energy state of a material. Moreover, unlike high temperature, high pressure strongly suppresses atomic diffusion. Therefore, no compositional change is usually expected during the high-pressure tests at room temperature [63], which is also confirmed by the EDS results (Supplementary Fig. S2b) in this study. As shown in Table 1, the high pressure induced polymorphic transitions in pure elements, and traditional low-entropy alloys are usually reversible [5,7,26,31,37]. In contrast, the transitions in the Al06 HEA are irreversible. All the results suggest that severe lattice distortion may play a key role resulting in and stabilizing the rich polymorphism of the Al06 HEA. The lattice distortion is obvious in the *bct* phase compared with the *bcc* phases (Fig. 3). Supplementary Fig. S6 shows the comparison of the XRD curve of the orthorhombic phase in the gas-atomized Al06 and the *hcp* phase in the annealed Al06 at 40.4 GPa. The unconformity of these two curves further confirms that the orthorhombic phase is different to the *hcp* phase, and the former could be regarded as a distorted *hcp* with lower symmetry, which was hindered halfway to the *hcp* phase by lattice distortion. This transition stagnation is also consistent with the incomplete volume collapse as shown in Fig. 2a.

As previously discussed, the axis ratio *b/a* could correlate the orthorhombic phase with the *bcc/hcp* phase: *b/a* is $\sqrt{2}$ for the *bcc* phase and $\sqrt{3}$ for the *hcp* phase. Fig. 2b shows the *b/a* and *c/a* ratios variation in the gas-atomized original Al06 and *c/a* in the annealed Al06 during loading. The *c/a* ratio of the *hcp* phase in the annealed Al06 is almost constant at 1.62 ± 0.01 during loading, consistent with the previous works on the high-pressure *fcc*-to-*hcp* transitions in HEAs [62–65]. The *b/a* and *c/a* ratios of the orthorhombic phase continuously increase during the loading process, indicating that the orthorhombic phase keeps approaching the *hcp* phase with increasing pressure.

The local lattice distortion is inevitably introduced when an element is added into another solute lattice forming a solid solution, which typically makes plastic deformation more difficult and causes strengthening. This lattice distortion is believed to be more severe in the HEAs with multiprinciple elements [40–42] and has been extensively studied as a core effect of HEAs [56,60,61]. However, how the lattice distortion affects the phase stability and polymorphism has not been addressed before. One of the key factors that cause lattice distortion is the relative atomic size mismatch between the constituent elements in HEAs. High pressure has been proven to be an effective way to modulate the atomic size mismatch and therefore, tune the lattice distortion [76]. For the Al06 HEA, the Al atoms have the biggest atomic size but the lowest bulk modulus; therefore, its lattice distortion could be susceptible to pressure, which could be the reason for the unusually rich polymorphism observed in this study.

As shown in Fig. S3, the sample after high-pressure compression had been severely deformed. Plastic deformation is usually caused by shear stress which is over the shear strength of a material. Shear stress is a typical driving force for many displacive phase transitions. Shear stress (caused by the non-hydrostaticity of the pressure medium) has been found to depress the onset transition pressure of the pressure-induced *fcc* to *hcp* transition in CoCrFeNiMn HEA in a DAC. If no obvious shear stress is involved with helium as the pressure medium, the *fcc* to *hcp* transition was also observed in the CoCrFeNiMn HEA only with higher transition pressure of ~22 GPa [77]. However, pure shear stress (plastic deformation)−induced obvious phase transition has not been observed in the Al*x*CoCrFeNi HEAs or their close related HEAs at low (ambient) hydrostatic pressures. For example, the high-pressure torsion (HPT) and cold rolling (CR), which are two effective methods to induce severe plastic deformation in alloys by applying high shear stress, have been employed to study the Al*x*CoCrFeNi and CoCrFeNiMn HEA

Appendix A. Supplementary data

Supplementary data to this article can be found online at https://doi.org/10.1016/j.mtphys.2018.12.002.

systems [78–80]. After the HPT, grain refinement to nanocrystals was reported in the Al0.3CoCrFeNi [79] and CoCrFeNiMn [78] HEAs, but no obvious phase transition was found at room temperature. In the work of Kao et al., $Al_xCoCrFeNi$ ($0 \le x \le 2$) HEAs were cold rolled by a 50% reduction of thickness and no any phase transition was found as well [80]. The phase transitions observed in the Al06 HEA start at ~10 GPa in the current work. Around 10 GPa, silicone oil can still provide quite good hydrostatic condition [77], no obvious plastic deformation is expected to occur. Therefore, we believed that the lattice distortion tuned by high hydrostatic pressure, instead of the plastic deformation, play a dominant role in controlling the formation of various polymorphs in the Al06 HEA.

5. Conclusions

In conclusion, five polymorphs, including *bcc*, orthorhombic, *bct*, *fcc,* and *hcp* were observed in the Al06 HEA. It is unusual compared with the typical two or three polymorphs in the transition metal elements reported in a similar pressure and temperature synthesis/treatment region (Table 1). Moreover, all these five phases of Al06 HEA could exist/co-exist at ambient conditions. Our work suggests that the lattice distortion could alter the phase transition pathway and promote rich polymorphism in HEAs. Since multicomponents can be incorporated into a single lattice of an HEA and the composition space is basically infinite, the difference of the atomic size and bulk modulus between the constituent elements provides vast unexplored space for pressure and temperature to tune in HEAs. Therefore, the abundant polymorphic transitions discovered in this work are expected to be general in various HEAs.

Author contributions

Y.F.X., Q.S.Z., and Z.H.N. initiated this research project. Q.S.Z., Y.F.X., Z.H.N., and Liang W. designed the experiments. B.P.W and S.C.Z synthesized the initial sample. Q.S.Z., Z.D.Z., Liang W., H.B.L., and X.H.C. performed the synchrotron radiation X-ray experiments. F.Z. and B.Y.C performed the TEM work. Liang W., Q.S.Z., Y.F.X., Z.H.N., Y.R., and F.Z. analyzed the data. Liang W., Q.S.Z., and Y.F.X. wrote the paper. All authors participated in the discussions and commented on the manuscript.

Conflicts of interest

The authors declare no competing financial interests.

Data availability

The raw/processed data required to reproduce these findings cannot be shared at this time due to technical or time limitations.

Acknowledgment

References

[1] D.N. Polsin, D.E. Fratanduono, J.R. Rygg, A. Lazicki, R.F. Smith, J.H. Eggert, M.C. Gregor, B.H. Henderson, J.A. Delettrez, R.G. Kraus, P.M. Celliers, F. Coppari, D.C. Swift, C.A. McCoy, C.T. Seagle, J.P. Davis, S.J. Burns, G.W. Collins, T.R. Boehly, Measurement of body-centered-cubic aluminum at 475 GPa, Phys. Rev. Lett. 119 (2017) 175702. http://doi.org/10.1103/PhysRevLett.119.175702.

[2] Y. Lu, T. Sun, P. Zhang, P. Zhang, D.B. Zhang, R.M. Wentzcovitch, Premelting hcp to bcc transition in beryllium, Phys. Rev. Lett. 118 (2017) 145702. http://doi.org/10.1103/PhysRevLett.118.145702.

[3] R. Jaramillo, Y. Feng, J.C. Lang, Z. Islam, G. Srajer, H.M. Rønnow, P.B. Littlewood, T.F. Rosenbaum, Chromium at high pressures: weak coupling and strong fluctuations in an itinerant antiferromagnet, Phys. Rev. B Condens. Matter Mater. Phys. 77 (2008) 184418. http://doi.org/10.1103/PhysRevB.77.184418.

[4] A. Dewaele, C. Denoual, S. Anzellini, F. Occelli, M. Mezouar, P. Cordier, S. Merkel, M. Véron, E. Rausch, Mechanism of the α-ε phase transformation in iron, Phys. Rev. B Condens. Matter Mater. Phys. 91 (2015) 174105. http://doi.org/10.1103/PhysRevB.91.174105.

[5] K.K. Pandey, J. Gyanchandani, M. Somayazulu, G.K. Dey, S.M. Sharma, S.K. Sikka, Reinvestigation of high pressure polymorphism in hafnium metal, J. Appl. Phys. 115 (2014) 233513. http://doi.org/10.1063/1.4884436.

[6] L. Zhu, H. Wang, Y. Wang, J. Lv, Y. Ma, Q. Cui, Y. Ma, G. Zou, Substitutional alloy of Bi and Te at high pressure, Phys. Rev. Lett. 106 (2011) 145501. http://doi.org/10.1103/PhysRevLett.106.145501.

[7] L. Dubrovinsky, N. Dubrovinskaia, O. Narygina, I. Kantor, A. Kuznetzov, V.B. Prakapenka, L. Vitos, B. Johansson, A.S. Mikhaylushkin, S.I. Simak, I.A. Abrikosov, Body-centered cubic iron-nickel alloy in earth's core, Science 316 (2007) 1880–1884. http://doi.org/10.1126/science.1142105.

[8] Y. Ding, R. Ahuja, J. Shu, P. Chow, W. Luo, H.K. Mao, Structural phase transition of vanadium at 69 GPa, Phys. Rev. Lett. 98 (2007) 085502. http://doi.org/10.1103/PhysRevLett.98.085502.

[9] Y. Akahama, M. Nishimura, K. Kinoshita, H. Kawamura, Y. Ohishi, Evidence of a fcc-hcp transition in aluminum at multimegabar pressure, Phys. Rev. Lett. 96 (2006) 045505. http://doi.org/10.1103/PhysRevLett.96.045505.

[10] R. Jaramillo, Y. Feng, J. Wang, T.F. Rosenbaum, Signatures of quantum criticality in pure Cr at high pressure, Proc. Natl. Acad. Sci. 107 (2010) 13631–13635. http://doi.org/10.1073/pnas.1005036107.

[11] Y. Feng, R. Jaramillo, J. Wang, Y. Ren, T.F. Rosenbaum, Invited Article, High-pressure techniques for condensed matter physics at low temperature, Rev. Sci. Instrum. 81 (2010) 041301. http://doi.org/10.1063/1.3400212.

[12] H.-K. Mao, W.A. Basset, T. Takahashi, Effect of pressure on crystal structure and lattice parameter of iron up to 300 kbar, J. Appl. Phys. 38 (1967) 1–6. http://doi.org/10.1063/1.1708965.

[13] M. Ueno, A. Onodera, O. Shimomura, K. Takemura, X-ray observation of the structural phase transition of aluminum nitride under high pressure, Phys. Rev. B 45 (1992) 10123–10126. http://doi.org/10.1103/PhysRevB.45.10123.

[14] S. Ono, T. Kikegawa, Y. Ohishi, High-pressure phase transition of hematite, Fe_2O_3, J. Phys. Chem. Solids. 65 (2004) 1527–1530. http://doi.org/10.1016/j.jpcs.2003.11.042.

[15] S. Asbrink, A. Waskowska, L. Gerward, J.S. Olsen, E. Talik, High-pressure phase transition and properties of spinel $ZnMn_2O_4$, Phys. Rev. B 60 (1999) 651–656. http://doi.org/10.1103/PhysRevB.60.12651.

[16] Y. Wang, J. Zhang, J. Wu, J.L. Coffer, Z. Lin, S. V Sinogeikin, W. Yang, Y. Zhao, Phase transition and compressibility in silicon nanowires, Nano Lett. 8 (2008) 2891–2895. http://doi.org/10.1021/nl8016576.

[17] L. Bai, Q. Li, S.A. Corr, M. Pravica, C. Chen, Y. Zhao, S.V. Sinogeikin, Y. Meng, C. Park, G. Shen, Pressure-induced cation-cation bonding in V_2O_3, Phys. Rev. B 92 (2015) 134106. http://doi.org/10.1103/PhysRevB.92.134106.

[18] Y. Wang, J. Zhu, W. Yang, T. Wen, M. Pravica, Z. Liu, M. Hou, Y. Fei, L. Kang, Z. Lin, C. Jin, Y. Zhao, Reversible switching between pressure-induced amorphization and thermal-driven recrystallization in $VO_2(B)$ nanosheets, Nat. Commun. 7 (2016) 12214. http://doi.org/10.1038/ncomms12214.

[19] H.K. Mao, J. Wu, L.C. Chen, J.F. Shu, Static compression of iron to 300 GPa and Fe(0.8)Ni(0.2) alloy to 260 GPa − implications for composition of the core, J. Geophys. Res. 95 (1990) 21737. http://doi.org/10.1029/JB095iB13p21737.

[20] Q. Zeng, Y. Ding, W.L. Mao, W. Yang, S.V. Sinogeikin, J. Shu, H. Mao, J.Z. Jiang, Origin of pressure-induced polyamorphism in Ce75Al25 metallic glass, Phys. Rev. Lett. 104 (2010) 105702. http://doi.org/10.1103/PhysRevLett.104.105702.

[21] L. Dubrovinsky, N. Dubrovinskaia, I.A. Abrikosov, M. Vennström, F. Westman, S. Carlson, M. van Schilfgaarde, B. Johansson, B. Johansson, Pressure-induced invar effect in Fe-Ni alloys, Phys. Rev. Lett. 86 (2001) 4851–4854. http://doi.org/10.1103/PhysRevLett.86.4851.

[22] B. Chen, J.-F. Lin, J. Chen, H. Zhang, Q. Zeng, Synchrotron-based high-pressure research in materials science, MRS Bull. 41 (2016) 473–478. http://doi.org/10.1557/mrs.2016.110.

[23] A.P. Drozdov, M.I. Eremets, I.A. Troyan, V. Ksenofontov, S.I. Shylin, Conventional superconductivity at 203 kelvin at high pressures in the sulfur hydride system, Nature 525 (2015) 73–76. http://doi.org/10.1038/nature14964.

[24] D.Y. Kim, R.H. Scheicher, H.K. Mao, T.W. Kang, R. Ahuja, General trend for pressurized superconducting hydrogen-dense materials, Proc. Natl. Acad. Sci. 107 (2010) 2793—2796. http://doi.org/10.1073/pnas.0914462107.

[25] P.M. Giles, M.H. Longenbach, A.R. Marder, High-pressure α-ε martensitic transformation in iron, J. Appl. Phys. 42 (1971) 4290—4295. http://doi.org/10.1063/1.1659768.

[26] C.S. Yoo, H. Cynn, P. Söderlind, V. Iota, New beta(fcc) -cobalt to 210 GPa, Phys. Rev. Lett. 84 (2000) 18—21. http://doi.org/10.1103/PhysRevLett.84.4132.

[27] H. Huang, Y. Wu, J. He, H. Wang, X. Liu, K. An, W. Wu, Z. Lu, Phase-transformation ductilization of brittle high-entropy alloys via metastability engineering, Adv. Mater. (2017) 1701678. http://doi.org/10.1002/adma.201701678.

[28] Z. Li, K.G. Pradeep, Y. Deng, D. Raabe, C.C. Tasan, Metastable high-entropy dual-phase alloys overcome the strength−ductility trade-off, Nature 534 (2016) 227. http://doi.org/10.1038/nature17981.

[29] G. Steinle-Neumann, L. Stixrude, R.E. Cohen, First-principles elastic constants for the hcp transition metals Fe, Co, and Re at high pressure, Phys. Rev. B Condens. Matter Mater. Phys. 60 (1999) 791—799. http://doi.org/10.1103/PhysRevB.60.791.

[30] A. Dewaele, P. Loubeyre, F. Occelli, M. Mezouar, P.I. Dorogokupets, M. Torrent, Quasihydrostatic equation of state of iron above 2 Mbar, Phys. Rev. Lett. 97 (2006) 215504. http://doi.org/10.1103/PhysRevLett.97.215504.

[31] W.A. Bassett, E. Huang, Mechanism of the body-centered cubic-hexagonal close-packed phase transition in iron, Science 238 (1987) 780—783. http://doi.org/10.1126/science.238.4828.780.

[32] F. Wang, R. Ingalls, Iron bcc-hcp transition: local structure from x-ray-absorption fine structure, Phys. Rev. B 57 (1998) 5647—5654. http://doi.org/10.1103/PhysRevB.57.5647.

[33] D.H. Kalantar, J.F. Belak, G.W. Collins, J.D. Colvin, H.M. Davies, J.H. Eggert, T.C. Germann, J. Hawreliak, B.L. Holian, K. Kadau, P.S. Lomdahl, H.E. Lorenzana, M.A. Meyers, K. Rosolankova, M.S. Schneider, J. Sheppard, J.S. Stolken, J.S. Wark, Direct observation of the α-ε transition in shock-compressed iron via nanosecond X-ray diffraction, Phys. Rev. Lett. 95 (2005) 075502. http://doi.org/10.1103/PhysRevLett.95.075502.

[34] N. Amadou, T. De Resseguier, E. Brambrink, T. Vinci, A. Benuzzi-Mounaix, G. Huser, G. Morard, F. Guyot, K. Miyanishi, N. Ozaki, R. Kodama, M. Koenig, Kinetics of the iron α-ε phase transition at high-strain rates: experiment and model, Phys. Rev. B 93 (2016) 214108. http://doi.org/10.1103/PhysRevB.93.214108.

[35] H. Xia, S.J. Duclos, A.L. Ruoff, Y.K. Vohra, New high-pressure phase transition in zirconium metal, Phys. Rev. Lett. 64 (1990) 204—207. http://doi.org/10.1103/PhysRevLett.64.204.

[36] Y.K. Vohra, P.T. Spencer, Novel γ-phase of titanium metal at megabar pressures, Phys. Rev. Lett. 86 (2001) 3068—3071. http://doi.org/10.1103/PhysRevLett.86.3068.

[37] A. Jayaraman, W. Klement, G.C. Kennedy, Solid-solid transitions in titanium and zirconium at high pressures, Phys. Rev. 131 (1963) 644—649. http://doi.org/10.1103/PhysRev.131.644.

[38] P. Tolédano, G. Krexner, M. Prem, M. Prem, H.P. Weber, V.P. Dmitriev, Theory of the martensitic transformation in cobalt, Phys. Rev. B Condens. Matter Mater. Phys. 64 (2001) 144104. http://doi.org/10.1103/PhysRevB.64.144104.

[39] A. Mujica, A. Rubio, A. Muñoz, R.J. Needs, High-pressure phases of group-IV, III-V, and II-VI compounds, Rev. Mod. Phys. 75 (2003) 863—912. http://doi.org/10.1103/RevModPhys.75.863.

[40] H.P. Chou, Y.S. Chang, S.K. Chen, J.W. Yeh, Microstructure, thermophysical and electrical properties in AlxCoCrFeNi (0≤x ≤2) high-entropy alloys, Mater. Sci. Eng. B Solid State Mater. Adv. Technol. 163 (2009) 184—189. http://doi.org/10.1016/j.mseb.2009.05.024.

[41] Y.F. Ye, Q. Wang, J. Lu, C.T. Liu, Y. Yang, High-entropy alloy: challenges and prospects, Mater. Today 19 (2016) 349—362. http://doi.org/10.1016/j.mattod.2015.11.026.

[42] Y. Zhang, T.T. Zuo, Z. Tang, M.C. Gao, K.A. Dahmen, P.K. Liaw, Z.P. Lu, Microstructures and properties of high-entropy alloys, Prog. Mater. Sci. 61 (2014) 1—93. http://doi.org/10.1016/j.pmatsci.2013.10.001.

[43] J.W. Yeh, S.K. Chen, S.J. Lin, J.Y. Gan, T.S. Chin, T.T. Shun, C.H. Tsau, S.Y. Chang, Nanostructured high-entropy alloys with multiple principal elements: novel alloy design concepts and outcomes, Adv. Eng. Mater. 6 (2004) 299—303. http://doi.org/10.1002/adem.200300567.

[44] B. Gludovatz, A. Hohenwarter, D. Catoor, E.H. Chang, E.P. George, R.O. Ritchie, A fracture-resistant high-entropy alloy for cryogenic applications, Science 345 (2014) 1153—1158. http://doi.org/10.1126/science.1254581.

[45] O.N. Senkov, J.M. Scott, S.V. Senkova, D.B. Miracle, C.F. Woodward, Microstructure and room temperature properties of a high-entropy TaNbHfZrTi alloy, J. Alloys Compd. 509 (2011) 6043—6048. http://doi.org/10.1016/j.jallcom.2011.02.171.

[46] M. Feuerbacher, M. Heidelmann, C. Thomas, Hexagonal high-entropy alloys, Mater. Res. Lett. 3 (2014) 1—6. http://doi.org/10.1080/21663831.2014.951493.

[47] B. Cantor, I.T.H. Chang, P. Knight, A.J.B. Vincent, Microstructural development in equiatomic multicomponent alloys, Mater. Sci. Eng. A 375−377 (2004) 213—218. http://doi.org/10.1016/j.msea.2003.10.257.

[48] Z. Wu, H. Bei, G.M. Pharr, E.P. George, Temperature dependence of the mechanical properties of equiatomic solid solution alloys with face-centered cubic crystal structures, Acta Mater. 81 (2014) 428—441. http://doi.org/10.1016/j.actamat.2014.08.026.

[49] C.Y. Hsu, T.S. Sheu, J.W. Yeh, S.K. Chen, Effect of iron content on wear behavior of AlCoCrFexMo0.5Ni high-entropy alloys, Wear 268 (2010) 653—659. http://doi.org/10.1016/j.wear.2009.10.013.

[50] M.A. Hemphill, T. Yuan, G.Y. Wang, J.W. Yeh, C.W. Tsai, A. Chuang, P.K. Liaw, Fatigue behavior of Al0.5CoCrCuFeNi high entropy alloys, Acta Mater. 60 (2012) 5723—5734. http://doi.org/10.1016/j.actamat.2012.06.046.

[51] P.J.S. Buenconsejo, H.Y. Kim, H. Hosoda, S. Miyazaki, Shape memory behavior of Ti-Ta and its potential as a high-temperature shape memory alloy, Acta Mater. 57 (2009) 1068—1077. http://doi.org/10.1016/j.actamat.2008.10.041.

[52] Z.W. Zhu, C.Y. Xiong, J. Wang, R.G. Li, Y. Ren, Y.D. Wang, Y. Li, In situ synchrotron X-ray diffraction investigations of the physical mechanism of ultra-low strain hardening in Ti-30Zr-10Nb alloy, Acta Mater. 154 (2018) 45—55. http://doi.org/10.1016/j.actamat.2018.05.034.

[53] F. Otto, A. Dlouhý, C. Somsen, H. Bei, G. Eggeler, E.P. George, The influences of temperature and microstructure on the tensile properties of a CoCrFeMnNi high-entropy alloy, Acta Mater. 61 (2013) 5743—5755. http://doi.org/10.1016/j.actamat.2013.06.018.

[54] U. Sydney, A. Hohenwarter, A fracture-resistant high-entropy alloy for cryogenic applications, Science 345 (2014) 1153—1159. http://doi.org/10.1126/science.1254581.

[55] A. Haglund, M. Koehler, D. Catoor, E.P. George, V. Keppens, Polycrystalline elastic moduli of a high-entropy alloy at cryogenic temperatures, Intermetallics 58 (2015) 62—64. http://doi.org/10.1016/j.intermet.2014.11.005.

[56] H.S. Oh, D. Ma, G.P. Leyson, B. Grabowski, E.S. Park, F. Kormann, D. Raabe, Lattice distortions in the FeCoNiCrMn high entropy alloy studied by theory and experiment, Entropy 18 (2016) 321. http://doi.org/10.3390/e18090321.

[57] W.H. Liu, Y. Wu, J.Y. He, T.G. Nieh, Z.P. Lu, Grain growth and the Hall-Petch relationship in a high-entropy FeCrNiCoMn alloy, Scr. Mater. 68 (2013) 526—529. http://doi.org/10.1016/j.scriptamat.2012.12.002.

[58] K.Y. Tsai, M.H. Tsai, J.W. Yeh, Sluggish diffusion in Co-Cr-Fe-Mn-Ni high-entropy alloys, Acta Mater. 61 (2013) 4887—4897. http://doi.org/10.1016/j.actamat.2013.04.058.

[59] Z. Wang, H. Huang, Y. Yang, J. Wang, C.T. Liu, Atomic-size effect and solid solubility of multicomponent alloys, Scr. Mater. 94 (2015) 28—31. http://doi.org/10.1016/j.scriptamat.2014.09.010.

[60] Z. Wang, W. Qiu, Y. Yang, C.T. Liu, Atomic-size and lattice-distortion effects in newly developed high-entropy alloys with multiple principal elements, Intermetallics 64 (2015) 63—69. http://doi.org/10.1016/j.intermet.2015.04.014.

[61] H. Song, F. Tian, Q.-M. Hu, L. Vitos, Y. Wang, J. Shen, N. Chen, Local lattice distortion in high-entropy alloys, Phys. Rev. Mater. 1 (2017) 023404. http://doi.org/10.1103/PhysRevMaterials.1.023404.

[62] C.L. Tracy, S. Park, D.R. Rittman, S.J. Zinkle, H. Bei, M. Lang, R.C. Ewing, W.L. Mao, High pressure synthesis of a hexagonal close-packed phase of the high-entropy alloy CrMnFeCoNi, Nat. Commun. 8 (2017) 15634. http://doi.org/10.1038/ncomms15634.

[63] F. Zhang, Y. Wu, H. Lou, Z. Zeng, V. Prakapenka, E. Greenberg, Y. Ren, Polymorphism in a high-entropy alloy, Nat. Commun. 8 (2017) 15687. http://doi.org/10.1038/ncomms15687.

[64] E.W. Huang, C.M. Lin, J. Jain, S.R. Shieh, C.P. Wang, Y.C. Chuang, Y.F. Liao, D.Z. Zhang, T. Huang, T.N. Lam, W. Woo, S.Y. Lee, Irreversible phase transformation in a CoCrFeMnNi high entropy alloy under hydrostatic compression, Mater. Today Commun. 14 (2018) 10—14. http://doi.org/10.1016/j.mtcomm.2017.12.001.

[65] F.X. Zhang, S. Zhao, K. Jin, H. Bei, D. Popov, C. Park, J.C. Neuefeind, W.J. Weber, Y. Zhang, Pressure-induced fcc to hcp phase transition in Ni-based high entropy solid solution alloys, Appl. Phys. Lett. 110 (2017) 011902. http://doi.org/10.1063/1.4973627.

[66] C. Prescher, V.B. Prakapenka, DIOPTAS: a program for reduction of two-dimensional X-ray diffraction data and data exploration, High Press. Res. 35 (2015) 223—230. http://doi.org/10.1080/08957959.2015.1059835.

[67] B.H. Toby, EXPGUI, a graphical user interface for GSAS, J. Appl. Crystallogr. 34 (2001) 210—213. http://doi.org/10.1107/S0021889801002242.

[68] D. Andrault, G. Fiquet, M. Kunz, F. Visocekas, D. Hausermann, The orthorhombic structure of iron: an in situ\study at high-temperature and high-pressure, Science 278 (1997) 831—834. http://doi.org/10.1126/science.278.5339.831.

[69] Y.L. Zhou, M. Niinomi, T. Akahori, Effects of Ta content on Young's modulus and tensile properties of binary Ti-Ta alloys for biomedical applications, Mater. Sci. Eng. A 371 (2004) 283—290. http://doi.org/10.1016/j.msea.2003.12.011.

[70] S. Zhou, P. Zhang, Y. Xue, F. Wang, L. Wang, T. Cao, Z. Tan, B. Cheng, B. Wang, Microstructure evolution of Al0.6CoCrFeNi high entropy alloy powder prepared by high pressure gas atomization, Trans. Nonferrous Met. Soc. China 28 (2018) 939—945. http://doi.org/10.1016/S1003-6326(18)64728-4.

[71] L. Wang, J.W. Qiao, S.G. Ma, Z.M. Jiao, T.W. Zhang, G. Chen, D. Zhao, Y. Zhang, Z.H. Wang, Mechanical response and deformation behavior of Al0.6CoCrFeNi high-entropy alloys upon dynamic loading, Mater. Sci. Eng. A 727 (2018) 208—213. http://doi.org/10.1016/j.msea.2018.05.001.

[72] L. Ma, L. Wang, Z. Nie, F. Wang, Y. Xue, J. Zhou, T. Cao, Y. Wang, Y. Ren, Reversible deformation-induced martensitic transformation in Al0.6CoCrFeNi high-entropy alloy investigated by in situ synchrotron-based high-energy X-ray diffraction, Acta Mater. 128 (2017) 12—21. http://doi.org/10.1016/j.actamat.2017.02.014.

[73] F. Birch, Elasticity and constitution of the Earth's interior, J. Geophys. Res. 57 (1952) 227—286. http://doi.org/10.1029/JZ057i002p00227.

[74] F. Tian, L.K. Varga, J. Shen, L. Vitos, Calculating elastic constants in high-entropy alloys using the coherent potential approximation: current issues and errors, Comput. Mater. Sci. 111 (2016) 350—358. http://doi.org/10.1016/j.commatsci.2015.09.058.

[75] D.B. Miracle, O.N. Senkov, A critical review of high entropy alloys and related concepts, Acta Mater. 122 (2017) 448—511. http://doi.org/10.1016/j.actamat.2016.08.081.

[76] Q.S. Zeng, Y. Ding, W.L. Mao, W. Luo, A. Blomqvist, R. Ahuja, W. Yang, J. Shu, S.V. Sinogeikin, Y. Meng, D.L. Brewe, J.Z. Jiang, H.K. Mao, Substitutional alloy of Ce and Al, Proc. Natl. Acad. Sci. 106 (2009) 2515—2518. http://doi.org/10.1073/pnas.0813328106.

[77] F. Zhang, H. Lou, S. Chen, X. Chen, Z. Zeng, J. Yan, W. Zhao, Y. Wu, Z. Lu, Q. Zeng, Effects of non-hydrostaticity and grain size on the pressure-induced phase transition of the CoCrFeMnNi high-entropy alloy, J. Appl. Phys. 115901 (2018). http://doi.org/10.1063/1.5046180.

[78] D.H. Lee, I.C. Choi, M.Y. Seok, J. He, Z. Lu, J.Y. Suh, M. Kawasaki, T.G. Langdon, J. Il Jang, Nanomechanical behavior and structural stability of a nanocrystalline CoCrFeNiMn high-entropy alloy processed by high-pressure torsion, J. Mater. Res. 30 (2015) 2804—2815. http://doi.org/10.1557/jmr.2015.239.

[79] Q.H. Tang, Y. Huang, Y.Y. Huang, X.Z. Liao, T.G. Langdon, P.Q. Dai, Hardening of an Al0.3CoCrFeNi high entropy alloy via high-pressure torsion and thermal annealing, Mater. Lett. 151 (2015) 126—129. http://doi.org/10.1016/j.matlet.2015.03.066.

[80] Y.F. Kao, T.J. Chen, S.K. Chen, J.W. Yeh, Microstructure and mechanical property of as-cast, -homogenized, and -deformed AlxCoCrFeNi ($0 \leq x \leq 2$) high-entropy alloys, J. Alloys Compd. 488 (2009) 57—64. http://doi.org/10.1016/j.jallcom.2009.08.090.

[81] M. Hanfland, I. Loa, K. Syassen, Sodium under pressure: Bcc to fcc structural transition and pressure-volume relation to 100 GPa, Phys. Rev. B Condens. Matter Mater. Phys. 65 (2002) 184109. http://doi.org/10.1103/PhysRevB.65.184109.

[82] T. Takahashi, H.K. Mao, W.A. Bassett, Lead: X-ray diffraction study of a high-pressure polymorph, Science 165 (1968) 1352—1353. http://doi.org/10.1126/science.165.3900.1352.

[83] S.B. Qadri, E.F. Skelton, A.W. Webb, High pressure studies of Ge using synchrotron radiation, J. Appl. Phys. 54 (1983) 3609—3611. http://doi.org/10.1063/1.332434.